Florida International University

FIU Digital Commons

5-2-2019

Intensified inundation shifts a freshwater wetland from a CO2 sink to a source

Junbin Zhao

Sparkle L. Malone

Steve F. Oberbauer

Paulo Olivas

Jessica L. Schedlbauer

See next page for additional authors

Authors

Junbin Zhao, Sparkle L. Malone, Steve F. Oberbauer, Paulo Olivas, Jessica L. Schedlbauer, Christina L. Staudhammer, and Gregory Starr

PRIMARY RESEARCH ARTICLE

Global Change Biology WILEY

Intensified inundation shifts a freshwater wetland from a CO$_2$ sink to a source

Junbin Zhao[1,2] ID | Sparkle L. Malone[1] ID | Steven F. Oberbauer[1] | Paulo C. Olivas[1,3] | Jessica L. Schedlbauer[1,4] | Christina L. Staudhammer[5] | Gregory Starr[5] ID

[1]Department of Biological Sciences and Southeast Environmental Research Center, Florida International University, Miami, Florida

[2]Division of Environment and Natural Resources, Department of Terrestrial Ecology, Norwegian Institute of Bioeconomy Research, Ås, Norway

[3]GIS-RS Center, Florida International University, Miami, Florida

[4]Department of Biology, West Chester University, West Chester, Pennsylvania

[5]Department of Biological Sciences, University of Alabama, Tuscaloosa, Alabama

Correspondence
Junbin Zhao, Division of Environment and Natural Resources, Department of Terrestrial Ecology, Norweigian Institute of Bioeconomy Research, Ås, Norway.
Email: junbinzhao1985@gmail.com

Funding information
U.S. Department of Energy, Grant/Award Number: 07-SC-NICCR-1059; Florida Coastal Everglades Long Term Ecological Research Program (FCE-LTER), Grant/Award Number: DBI-0620409 and DEB-1237517; National Science Foundation, Grant/Award Number: 1561139, 1233006 and 1807533

Abstract

Climate change has altered global precipitation patterns and has led to greater variation in hydrological conditions. Wetlands are important globally for their soil carbon storage. Given that wetland carbon processes are primarily driven by hydrology, a comprehensive understanding of the effect of inundation is needed. In this study, we evaluated the effect of water level (WL) and inundation duration (ID) on carbon dioxide (CO$_2$) fluxes by analysing a 10-year (2008–2017) eddy covariance dataset from a seasonally inundated freshwater marl prairie in the Everglades National Park. Both gross primary production (GPP) and ecosystem respiration (ER) rates showed declines under inundation. While GPP rates decreased almost linearly as WL and ID increased, ER rates were less responsive to WL increase beyond 30 cm and extended inundation periods. The unequal responses between GPP and ER caused a weaker net ecosystem CO$_2$ sink strength as inundation intensity increased. Eventually, the ecosystem tended to become a net CO$_2$ source on a daily basis when either WL exceeded 46 cm or inundation lasted longer than 7 months. Particularly, with an extended period of high-WLs in 2016 (i.e., WL remained >40 cm for >9 months), the ecosystem became a CO$_2$ source, as opposed to being a sink or neutral for CO$_2$ in other years. Furthermore, the extreme inundation in 2016 was followed by a 4-month postinundation period with lower net ecosystem CO$_2$ uptake compared to other years. Given that inundation plays a key role in controlling ecosystem CO$_2$ balance, we suggest that a future with more intensive inundation caused by climate change or water management activities can weaken the CO$_2$ sink strength of the Everglades freshwater marl prairies and similar wetlands globally, creating a positive feedback to climate change.

KEYWORDS
ecosystem respiration, flooding, gross primary production, hydrology, net ecosystem CO$_2$ exchange, wetland

1 | INTRODUCTION

Climate change has altered global precipitation patterns, resulting in significant changes in regional hydrology and increasing the frequency and intensity of both seasonal and episodic drought or flooding (IPCC, 2013). Ecosystem processes, especially those associated with greenhouse gas emissions (e.g., carbon dioxide), are highly sensitive to these alterations in hydrology and, in turn, may provide feedbacks to ongoing climate change. While many studies have focused on the effect of drought on ecosystem carbon dioxide (CO_2) exchange (e.g., Fenner & Freeman, 2011; Malone, Starr, Staudhammer, & Ryan, 2013; Rocha & Goulden, 2010; Taylor, Ripley, Woodward, & Osborne, 2011), less effort has been made to understand the effect of inundation (Han et al., 2015; Larmola et al., 2004; Morison et al., 2000).

Inundation is especially crucial in wetlands ecosystems, where CO_2 exchange and carbon sink potential are mainly driven by hydrology (Davis & Ogden, 1994). Wetlands have significant soil carbon pools (Kayranli, Scholz, Mustafa, & Hedmark, 2010). As climate change continues to shift precipitation patterns and, therefore, hydrology, the fate of wetland carbon becomes more uncertain (Burkett & Kusler, 2000; Erwin, 2009). Thus, there is an important need to understand how the ecosystem CO_2 balance, and its underlying processes, respond to changes in hydrological conditions, such as inundation regimes.

Inundation creates an anoxic soil environment that imposes different levels of physiological stress on wetland plants depending on their tolerances (Kozlowski, 1984; Pezeshki, 2001; Zhao, Oberbauer, et al., 2018). This stress usually results in declines in plant photosynthesis (Pezeshki, 2001; Zhao, Oberbauer, et al., 2018), which, consequently, reduces ecosystem CO_2 uptake. At the same time, stress induced by inundation also decreases ecosystem CO_2 emission by restraining plant autotrophic respiration (Bragina, Drozdova, Ponomareva, Alekhin, & Grineva, 2002; Gleason & Dunn, 1982; Islam & Macdonald, 2004). Sustained inundation can also limit the decomposition activities of soil microbes and reduce CO_2 emission from heterotrophic respiration (Anderson & Smith, 2002; Conner & Day, 1991; Fenner & Freeman, 2011; Happelll & Chanton, 1993; but see Zona et al., 2012). These changes between CO_2 uptake and emission are usually unequal, which can lead to significant shifts in the ecosystem CO_2 balance.

At the ecosystem level, the effect of inundation on net ecosystem CO_2 exchange (NEE) is determined by the difference between gross primary production (GPP; CO_2 uptake) and ecosystem respiration (ER; CO_2 emission). Previous wetland studies reported stronger reductions in GPP than that of ER during the inundation period, weakening the ecosystem CO_2 sink strength (Han et al., 2015; Schedlbauer, Oberbauer, Starr, & Jimenez, 2010). In contrast, enhanced CO_2 sink strength was found under higher water levels (WL) in an Amazon floodplain due to greater reductions in ER than GPP (Morison et al., 2000). Based on data collected from different wetland sites, Larmola et al. (2004) suggested that the effect of inundation on NEE can vary based on the dominant plant species. To date, the effect of inundation has mostly been studied as a binary or discrete factor (e.g., inundated vs. noninundated or high vs. low WL). To better understand the effect of inundation, a comprehensive picture of how continuous variation in hydrology, in terms of WL depth and inundation duration (ID), affects NEE and its components (i.e., GPP and ER) is still needed.

Furthermore, inundation may have legacy effects on CO_2 fluxes, such that effects extend into the season after inundation. For example, studies found that plant photosynthesis and growth can be suppressed for a period of time after inundation as vegetation recovers from the physiological stresses (Chen, Zamorano, & Ivanoff, 2010; Hu, Wu, Yao, & Xu, 2015; Kozlowski & Pallardy, 1979). Accordingly, lower net ecosystem CO_2 uptake was often noted following extensive inundation (Dušek et al., 2009; Hu et al., 2015). Therefore, to fully understand the influences of inundation on the ecosystem CO_2 budget, it is also important to evaluate these carryover effects of inundation and determine the length of their impact.

In the Florida Everglades, hydrology (i.e., inundation) plays a critical role in determining wetland types by affecting the plant species composition (Davis & Ogden, 1994; Todd et al., 2010). Of particular interest is the short-hydroperiod freshwater wetland ecosystem (sometimes referred to as marl prairies), which has seasonally alternating dry periods and inundation that fluctuates substantially with precipitation patterns (Davis & Ogden, 1994; Schedlbauer et al., 2010). This ecosystem has been shown to be a sink or neutral for annual CO_2 budgets (Jimenez et al., 2012; Malone, Staudhammer, Oberbauer, et al., 2014; Schedlbauer et al., 2010). The water depth and ID are the two variables that characterize the inundation intensity (Childers et al., 2006; Todd et al., 2010). Although previous studies have recognized that carbon dynamics of the ecosystem are driven by the seasonal inundation, how changes in water depth and ID interactively affect the underlying CO_2 fluxes is largely unknown.

In 2015–2017, due to a combination of extremely high precipitation at the end of 2015 and the beginning of 2016 (Figure S1), associated with El Niño Southern Oscillation (ENSO), and water management activities (i.e., greatly increased freshwater flow in an adjacent canal), the short-hydroperiod freshwater wetland (with an average inundation of ~6 months) in the eastern Everglades experienced an extended inundation period lasting for 17 months. This extreme event allowed us to test ecosystem response to inundation scenarios which were out of the normal range for this system but may occur more frequently in the future. In this study, we used eddy covariance (EC) data and the normalized difference vegetation index (NDVI; 2008–2017) from a site in the Everglades short-hydroperiod freshwater wetland to answer the following questions: (a) How do changes in water depth and ID affect the components of ecosystem CO_2 flux (i.e., NEE, GPP and ER)? (b) How does extreme inundation change the sink/source capacity of the ecosystem? (c) Does extreme inundation has lag effects on ecosystem CO_2 dynamics during the following seasons? Answering these questions can improve our current understanding of the influences of hydrologic shifts on the carbon dynamics of freshwater wetland ecosystems and inform the

processes needed for accurate representation of wetlands in ecosystem and Earth-system models.

2 | MATERIALS AND METHODS

2.1 | Site description

This study was carried out in a short-hydroperiod oligotrophic freshwater marl prairie (25°26′16.5″ N, 80°35′40.68″ W, elevation: ~1 m above sea level) near the headwaters of Taylor Slough on the eastern edge of Everglades National Park (Figure 1). The mean annual temperature is 23.9°C, with the average monthly temperature being lowest in January and highest in August (18.1°C and 29.4°C, respectively) (Jimenez et al., 2012). The site experiences a significant seasonal variation in irradiance and daily net radiation ranges from 6 to ~20 MJ m^{-2} day^{-1} (Malone, Staudhammer, Loescher, et al., 2014). The photosynthetically active radiation (PAR) reaches up to 2,350 µmol m^{-2} s^{-1} in April/May and up to 1,500 µmol m^{-2} s^{-1} in December/January. Annual precipitation averages 1,380 mm, ~70% of which occurs during June–November (Davis & Ogden, 1994). The hydrology of the site is also influenced by the comprehensive everglades restoration plan (Perry, 2004), which aims to improve the freshwater availability in the Everglades.

As a result of seasonal precipitation and water management activities affecting WL in an adjacent canal, the study site is inundated (i.e., WL exceeds soil surface level) for 4–6 months each year with WLs reaching 20–50 cm above the soil surface (Figure 2c). The surface water flows through the site from the north at a slow rate (0.5–0.8 cm/s) (Schaffranek & Ball, 2000) and the overall lateral carbon balance within the water is likely close to zero (Schedlbauer et al., 2010). The site is not impacted by salinity and has an ~14 cm layer of marl soils on top of limestone bedrock (Schedlbauer et al., 2010). The vegetation has a height of ~0.73 m and is codominated by the macrophytes sawgrass (*Cladium jamaicense* Crantz) and muhly grass (*Muhlenbergia filipes* M.A. Curtis) (Schedlbauer et al., 2010). Periphyton, which consists of algae, fungi, and bacteria, also develops progressively at the site during the inundated period as floating mats, benthic carpets, and "sweaters" around submerged macrophyte stems/leaves.

2.2 | Eddy covariance and meteorological instrumentation

An EC tower, which is a part of the AmeriFlux network, was established at the site in the fall of 2007. The EC system is composed of an open-path infrared gas analyzer (IRGA; LI-7500; LI-COR Inc., Lincoln,
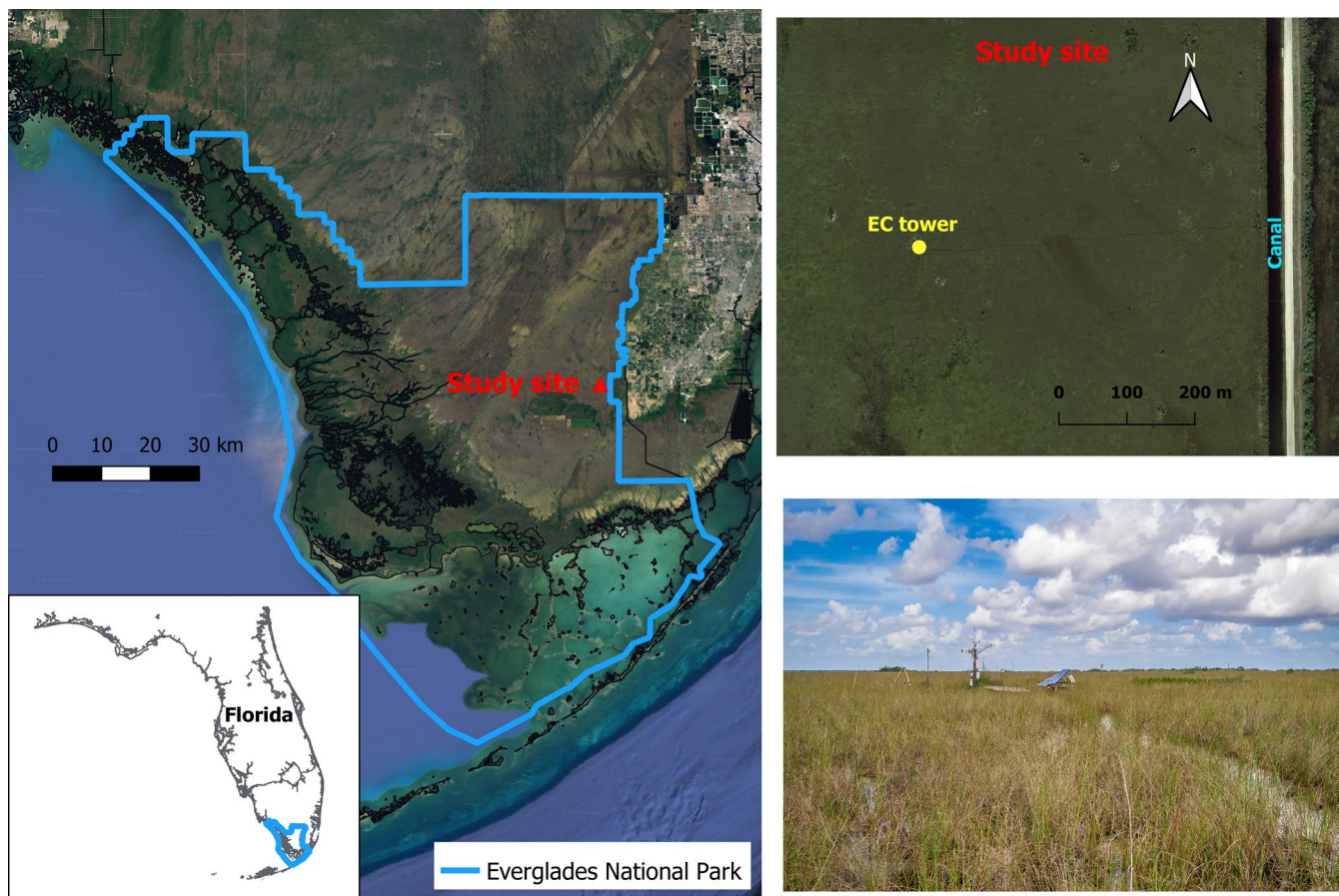
FIGURE 1 The location and landscape of the study site in a short-hydroperiod freshwater wetland on the eastern edge of the Everglades National Park (photo credit: Junbin Zhao)
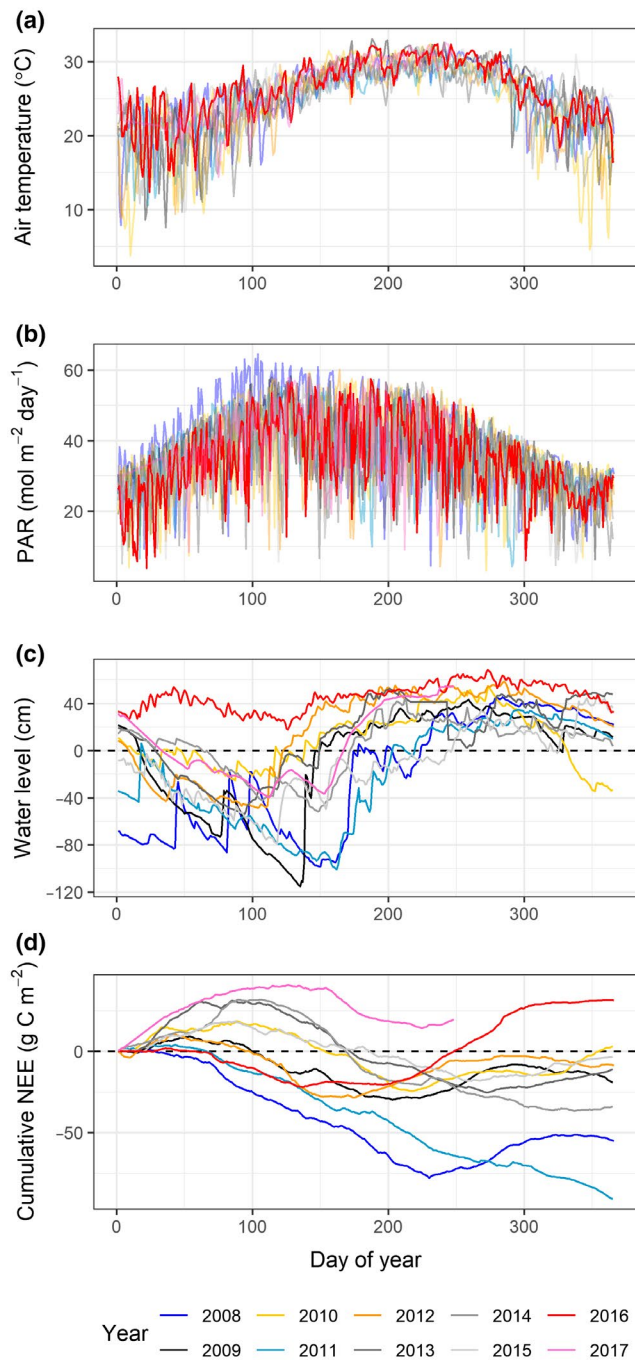
FIGURE 2 Seasonal variations of the daily mean air temperature (a), photosynthetically active radiation (PAR) sum (b), water level (WL) (c), and cumulative net ecosystem CO_2 exchange (NEE) (d) during 2008–2017. In (c), a negative value indicates a WL that is below the soil surface while a positive value indicates the WL is above the soil surface

NE, USA) that measures CO_2 and water vapor concentration and a 3-D sonic anemometer (CSAT3; Campbell Scientific Inc., Logan, UT, USA) that measures wind speed and air temperature. The instruments were installed 3.3 m above the ground. A CR1000 data logger (Campbell Scientific Inc.) was used to record the EC data at a frequency of 10 Hz.

The IRGA was calibrated monthly according to manufacturer instructions against standard calibration gases (i.e., nitrogen gas with soda lime and Drierite, 492.6 ppm CO_2 gas, and gas from a dewpoint generator; LI-610, LI-COR Inc.). The EC system was estimated to have a 90% fetch distance within 200 m of the tower (Schedlbauer et al., 2010; Zhao, Olivas, et al., 2018), an area that represents typical vegetation in the marl prairie with minimum impact from the adjacent canal (~400 m away, Figure 1).

For the meteorological variables used in our analysis, PAR was measured using a PARlite quantum sensor (Kipp & Zonen Inc., Delft, The Netherlands), and precipitation was measured by a tipping bucket rain gauge (TE525; Texas Electronics Inc., Dallas, TX, USA). The PAR and precipitation data were logged by a CR10X data logger (Campbell Scientific Inc.) every 15 s and their 30 min average and sum, respectively, were recorded. Water level was recorded every 30 min with a WL logger (HOBO U20-001-01; Onset, Bourne, MA, USA). More details on instrument setup are outlined in Jimenez et al. (2012), Malone, Staudhammer, Loescher, et al. (2014), Malone, Staudhammer, Oberbauer, et al. (2014) and Schedlbauer et al. (2010).

2.3 | Data processing

Eddy covariance data from January 1, 2008 to September 5, 2017 were used in this study. We calculated 30 min NEE from 10 Hz EC data with the program EdiRe (University of Edinburgh, http://www.geos.ed.ac.uk/abs/research/micromet/EdiRe) following protocols including coordinate rotation, despiking and air density corrections (Aubinet et al., 2000; Baldocchi, Hicks, & Meyers, 1988; Webb, Pearman, & Leuning, 1980). In the process, canopy height was adjusted against the WL change during the inundation period. The CO_2 storage term was estimated according to Hollinger et al. (1994) and included in the 30 min NEE values. The sampling rates were checked by implementing spectral analysis on the raw data. To ensure quality, data satisfying the following criteria were removed: (a) evidence of rainfall, contamination (e.g., condensation, spider webs or bird fouling) in the sampling path of IRGA or sonic anemometer, (b) incomplete 30 min data during calibration or maintenance, (c) friction velocity ($u*$) <0.15 m/s (Goulden, Munger, Fan, Daube, & Wofsy, 1996) or (d) implausible values found in our data sets. Overall, 27% of daytime and 70% of nighttime NEE were removed over the study period.

To calculate CO_2 budgets, missing NEE data were gap-filled on a monthly basis using separate equations for day- and nighttime. For daytime (PAR ≥ 10 μmol m^{-2} s^{-1}), data were gap-filled using a hyperbolic equation as a function of PAR:

$$NEE = ER - \frac{\alpha \cdot PAR \cdot P_{max}}{\alpha \cdot PAR + P_{max}} \quad (1)$$

where parameters to be estimated are: α (apparent quantum efficiency), ER (ecosystem respiration rate, μmol m^{-2} s^{-1}), and P_{max} (maximum ecosystem CO_2 uptake rate, μmol m^{-2} s^{-1}). For nighttime (PAR < 10 μmol m^{-2} s^{-1}), NEE is comprised entirely of ER and an exponential equation was used for the gap-filling as a function of air temperature (T_a):

$$\text{NEE} = \text{ER} = R_0 \cdot \exp^{b \cdot T_a} \qquad (2)$$

where the parameters to be estimated are: R_0 (base respiration rate when air temperature is 0°C) and b (an empirical coefficient indicating the temperature sensitivity of the fluxes). Gap-filled data were only used for calculating CO_2 flux budgets. Because data from September 5 to November 29, 2017 were missing due to system outages caused by Hurricane Irma, the annual CO_2 budget of 2017 was excluded from the analyses.

Following gap-filling of missing data, 30 min ER was estimated via Equation (1), for daytime and via Equation (2) for nighttime. GPP was then calculated as:

$$\text{GPP} = \text{NEE} - \text{ER}. \qquad (3)$$

In this study, we used the atmospheric sign convention, where negative flux values indicate CO_2 uptake while positive values indicate CO_2 emission. More details regarding EC data processing are outlined in Jimenez et al. (2012), Malone, Staudhammer, Loescher, et al. (2014) and Malone, Staudhammer, Oberbauer, et al. (2014). The EC data are available through AmeriFlux (https://ameriflux.lbl.gov/).

2.4 | Vegetation indices

To explain the responses of CO_2 fluxes to inundation, values of the NDVI at the site were obtained from Moderate Resolution Imaging Spectroradiometer (MODIS), which represent the vegetation dynamics over the study period (2008–2017). The index is a part of the Level 3 product "MOD13Q1" available at 250 m resolution over 16-day compositing periods (Didan, 2015). The data were accessed from https://modis.ornl.gov on June 6, 2018 and cover a 250 × 250 m area centered on the EC tower. NDVI is sensitive to chlorophyll greenness (Huete et al., 2002) and represents a normalized ratio of the reflected near-infrared and red radiation from the land surface:

$$\text{NDVI} = \frac{\text{NIR} - \text{RED}}{\text{NIR} - \text{RED}} \qquad (4)$$

where NIR and RED are the surface reflectance factors for near-infrared and red bands, respectively, which correspond to wavelengths of 841–876 and 620–670 nm, respectively.

2.5 | Data analysis

In this study, inundation is indicated by WL >0 cm and inundation intensity refers to the WL and ID.

We used the nongap-filled 30 min data over the study period to fit the light response curve for GPP adapted from Equation (1) to derive the parameters α and P_{max} as following:

$$\text{GPP} = \frac{\alpha \cdot \text{PAR} \cdot P_{max}}{\alpha \cdot \text{PAR} + P_{max}}. \qquad (5)$$

At the same time, the temperature response curve (Equation 2) was used to derive the parameters R_0 and b for ER. Based on the light

and temperature response curves, we examined the interactive effect of WL and ID on the parameters of the curves by using a parameter prediction approach. Specifically, the light and temperature response curves were fit with the parameters (i.e., α, P_{max}, R_0, and b) replaced by linear functions of WL, ID, and the interaction term as follows:

$$\text{GPP} = \frac{(a_0 + a_1\text{WL} + a_2\text{ID} + a_3\text{WL}\cdot\text{ID}) \cdot \text{PAR} \cdot (b_0 + b_1\text{WL} + b_2\text{ID} + b_3\text{WL}\cdot\text{ID})}{(a_0 + a_1\text{WL} + a_2\text{Inun\_D} + a_3\text{WL}\cdot\text{ID}) \cdot \text{PAR} + (b_0 + b_1\text{WL} + b_2\text{ID} + b_3\text{WL}\cdot\text{ID})}$$
$$(6)$$

$$\text{ER} = (c_0 + c_1\text{WL} + c_2\text{ID} + c_3\text{WL}\cdot\text{ID}) \cdot \exp^{(d_0 + d_1\text{WL} + d_2\text{ID} + d_3\text{WL}\cdot\text{ID})\cdot T_a} \qquad (7)$$

where $a_0 - a_3$, $b_0 - b_3$, $c_0 - c_3$, and $d_0 - d_3$ are coefficients to be estimated, water level and inundation duration are indicated by WL and ID. Where interaction terms between WL and ID were not significant (i.e., the ER model, $p > 0.05$), we further examined the individual effect of WL and ID on the parameters (i.e., R_0 and b) by excluding the interaction terms. Data with WL <0 cm as well as gap-filled data were excluded in the models. To visualize the relationships of the models we plotted the least square mean predicted parameters (i.e., α, P_{max}, R_0, and b) against WL under different IDs.

To determine the effect of WL and ID on NEE, we fit a linear mixed model to daily NEE as a function of WL, ID, and their interaction term. A first-order autoregressive variance–covariance structure, AR (1), was also included in the model to account for the temporal autocorrelation among measurements taken in adjacent time periods. Based on this model, the compensation points (i.e., the values of WL and inundation that correspond to NEE = 0 g C m^{-2} day^{-1}) were calculated and their 95% confidence intervals were estimated by block bootstrapping (300 random bootstrap replicates).

To determine the importance of inundation on annual CO_2 budgets, we performed linear regressions, using hydrological factors (e.g., mean WL during inundation period, length of inundation period, etc.) as predictors of the annual budgets of flux components (i.e., GPP, ER, and NEE).

To reveal the vegetation response to inundation, we fit a linear mixed model to NDVI as a function of WL, ID, and their interaction term. A first-order autoregressive variance–covariance structure, AR (1), was also included in the model to account for the temporal autocorrelation among measurements in adjacent time periods. Individual effects of WL and inundation were further assessed by plotting bin-average of NDVI as a function of WL (from 0 to 70 cm at 5 cm intervals) and IDs (from 0 to 360 days at 30 day intervals), respectively. As aids for trend visualizations, smooth lines were added based on the nonparametric Local Polynomial Regression (LOESS) in the boxplots.

Lastly, to examine whether inundation effect on the CO_2 fluxes persists into the season following the inundation period, we compared the temporal changes of the parameters (i.e., α, P_{max}, R_0, and b) from the light and temperature response curves after inundation among the studied years. For this purpose, light (Equation 5) and temperature (Equation 2) response curves were fit to the nongap-filled data within 90 days after inundation with parameters replaced by a linear function of days after inundation (similar to Equations 6 and 7). The models were fit separately for each year (Table S2). To account for nonlinear temporal variations,

LOESS curves were used to represent the variation of daily NEE and NDVI during the postinundation periods and compared among years.

The light and temperature response models were fit using the nonlinear least squares function "nls" in the program R 3.5.0 (R Development Core Team, 2018). The linear mixed models accounting for temporal autocorrelation was carried out using the package "nlme" (Pinheiro, Bates, DebRoy, Sarkar, & R Development Core Team, 2013). Bootstrapping was performed using the "boot" package (Canty & Ripley, 2017). Graphs were made using the R package "ggplot2" (Wickham, 2016). All reported average values in this study are shown as mean ± SE, unless otherwise specified.

3 | RESULTS

3.1 | Seasonal variation in environmental conditions and annual NEE

Mean daily air temperature at the study site peaked in June–August (29.5 ± 0.2°C) while it was lowest from November to February (21.1 ± 0.4°C) (Figure 2a). Total daily PAR peaked during April–July (42.8 ± 0.5 mol m^{-2} day^{-1}) and was lowest from December to January (25.6 ± 0.6 mol m^{-2} day^{-1}) (Figure 2b). With the exception of 2016, the ecosystem was usually inundated from June to December with an average WL of 21 ± 3 cm in 2008–2017. From January–May the WL stayed below the soil surface at an average level of −31 ± 4 cm (Figure 2c). In 2016, WL remained above the soil surface for the entire year, and the level reached its highest point of 69 cm in September. Air temperature and PAR showed similar patterns in 2016 to other years.

The annual NEE budget ranged from −91 to 3 g C m^{-2} year^{-1} with a mean of −27 g C m^{-2} year^{-1} during 2008–2015 (Figure 2d, Table 1). However, in 2016, annual NEE was 32 g C m^{-2} year^{-1}, becoming a net CO$_2$ source; NEE switched from net CO$_2$ uptake in the early months of the year to net emissions from June to the end of the year. In 2017, cumulative NEE was positive before September; however, due to the missing data after September, no conclusions about the annual CO$_2$ budget can be drawn.

3.2 | Effects of WL and ID on GPP and ER

In the GPP models, the effect of WL on α and P_{max} depended on the length of inundation, as evidenced by the significant interaction terms (p < 0.01, Table 2). Specifically, a higher WL was associated with a higher apparent quantum efficiency (α) while extension of inundation period greatly restrained the magnitude of α by decreasing both the slopes and intercepts with changing WL (Figure 3a). In contrast, lower maximum ecosystem CO$_2$ uptake rates (P_{max}) were present at higher WLs (Figure 3b). Like α, the slopes and intercepts of the relationships between P_{max} and WL also decreased as inundation extended. Overall, the effect of WL on P_{max} was more notable as the ID was short. Once the ID approached 1 year, P_{max} became almost irresponsive to the change of WL and its magnitude was already rather low (<2.7 μmol m^{-2} s^{-1}).

TABLE 1 Summary of annual CO$_2$ fluxes at the study site during 2008–2016

Year	GPP	ER	NEE
2008	−559	504	−55
2009	−518	498	−20
2010	−466	469	3
2011	−622	531	−91
2012	−512	503	−9
2013	−448	436	−12
2014	−514	480	−34
2015	−579	576	−3
2016	−366	398	32

Abbreviations: GPP, gross primary production (g C m^{-2} year^{-1}); ER, ecosystem respiration (g C m^{-2} year^{-1}); NEE, net ecosystem CO$_2$ exchange (g C m^{-2} year^{-1}).

For ER, WL and ID did not exhibit a significant interactive effect on the parameters b and R_0 (p > 0.05, Table 2). When excluding the interactive effect, WL showed significant effects on the parameter R_0 (i.e., base respiration rate when air temperature is 0°C) (p < 0.01) but not on b (i.e., temperature sensitivity of ER) (p > 0.05) (Figure 3c,d, Table S1). In contrast, ID showed no significant effect on either R_0 or b (p > 0.05).

3.3 | Effects of WL and ID on daily NEE

The interaction between WL and inundation was also significant in the model for NEE (Table 2). Based on the model, the daily NEE was ~−0.51 g C m^{-2} day^{-1} as net CO$_2$ uptake when the site was not inundated (i.e., WL <0 cm and inundation = 0 day). As the WL increased to 45.6 cm (95% confidence interval: 41.5–51.6 cm), the ecosystem changed from a net CO$_2$ sink to source even at the start of inundation (i.e., ID = 1 day) (Figure 4). As the inundation period extended, the WL corresponding to the carbon compensation point (i.e., NEE = 0 g C m^{-2} day^{-1}) declined exponentially. As the inundation exceeded 214 days (95% confidence interval: 201–235 days), the ecosystem was a net CO$_2$ source regardless of the water depth.

3.4 | Interannual variation in CO$_2$ fluxes

Evaluating the interannual variation in CO$_2$ fluxes (Table 1), average WL during inundation periods showed a significant correlation with the annual GPP (R^2 = 0.48, p = 0.04, Figure 6a), but not with ER (R^2 = 0.39, p = 0.07, Figure 6b). Compared to the WL, the length of inundation period exhibited stronger relationships with both annual GPP (R^2 = 0.74, p < 0.01, Figure 5d) and ER (R^2 = 0.74, p < 0.01, Figure 5e). However, neither WL nor inundation period presented a significant correlation with annual NEE (R^2 ≤ 0.35, p = 0.10, Figure 5c,f). Instead, the relationship was only significant when examining annual NEE as a function of length of the period with WL >40 cm (R^2 = 0.48, p = 0.04, Figure 5i). The period with WL >40 cm was also significantly correlated with both annual GPP (R^2 = 0.69, p < 0.01, Figure 5g) and ER (R^2 = 0.55, p = 0.02, Figure 5h), but the explanatory power of these

TABLE 2 Summary of the models relating parameters from light (α, P_{max}), temperature (R_0, b) response curves, NEE, and NDVI to WL and ID

Parameter	Effect	Estimate	SE	t value
α	Intercept	-1.760×10^{-2}	1.185×10^{-3}	-14.849^{**}
	WL	-3.199×10^{-4}	5.260×10^{-5}	-6.084^{**}
	ID	8.500×10^{-6}	6.300×10^{-6}	1.340
	WL–ID	1.100×10^{-6}	2.000×10^{-7}	6.640^{**}
P_{max}	Intercept	-5.413	7.875×10^{-2}	-68.733^{**}
	WL	6.971×10^{-2}	2.339×10^{-3}	29.804^{**}
	ID	8.919×10^{-3}	3.852×10^{-4}	23.153^{**}
	WL–ID	-2.089×10^{-4}	1.110×10^{-5}	-18.874^{**}
R_0	Intercept	3.646×10^{-1}	2.654×10^{-2}	13.737^{**}
	WL	-5.453×10^{-4}	8.568×10^{-4}	-0.636
	ID	-1.470×10^{-5}	1.172×10^{-4}	-0.126
	WL–ID	-4.500×10^{-6}	2.900×10^{-6}	-1.553
b	Intercept	4.526×10^{-2}	2.517×10^{-3}	17.979^{**}
	WL	-1.669×10^{-4}	8.450×10^{-5}	-1.976^{*}
	ID	1.650×10^{-5}	1.290×10^{-5}	1.285
	WL–ID	5.000×10^{-7}	3.000×10^{-7}	1.568
NEE	Intercept	-5.098×10^{-1}	4.963×10^{-2}	-10.273^{**}
	WL	1.088×10^{-2}	1.616×10^{-3}	6.734^{**}
	ID	2.423×10^{-3}	2.743×10^{-4}	8.833^{**}
	WL–ID	-3.89×10^{-5}	7.15×10^{-6}	-5.443^{**}
NDVI	Intercept	4.914×10^{-1}	3.288×10^{-2}	14.943^{**}
	WL	-5.025×10^{-1}	9.755×10^{-2}	-5.151^{**}
	ID	3.860×10^{-5}	1.992×10^{-4}	0.194
	WL–ID	6.313×10^{-4}	4.811×10^{-4}	1.312

Abbreviations: ID, inundation duration (days); NDVI, normalized difference vegetation index; NEE, net ecosystem CO_2 exchange; WL, water level (cm). "WL–ID" indicates the interaction between WL and ID.
* and ** indicate the coefficient is significant at $p < 0.05$ and $p < 0.01$, respectively.

regressions was lower than those with the length of the entire inundation period as the independent variable (Figure 5d,e).

3.5 | Effects of WL and ID on NDVI

Normalized difference vegetation index showed a significant relationship with WL ($p < 0.01$) and this relationship was independent of the ID (Table 2). Moreover, this relationship tended to be nonlinear, where NDVI value remained at ~0.41 under a WL of 0–40 cm and declined to ~0.29 only when WL increased from 40 to 70 cm (Figure 6a). In contrast, the NDVI showed no consistent relationship with ID (Figure 6b).

## 3.6 | Postinundation CO_2 fluxes and NDVI

Based on the postinundation changes in parameters of the light response curves, a faster increase rate of α was found in first 3 months of 2017 after the extreme inundation event compared to other years (except 2014) (Figure 7a, Table S2). However, a relatively lower initial P_{max} together with a lower rate of increase was found in 2017 during the postinundation period compared to other years (Figure 7b). For the temperature response curves of ER, R_0 and b exhibited a decreasing

and an increasing trend, respectively, after inundation in 2017, which was similar to the years 2010, 2013, and 2015 (Figure 7c,d). However, a low initial temperature sensitivity ($b = 0.02$) was present in 2017 compared to other years (i.e., b ranged from 0.03 to 0.07) (Table S2).

Overall, compared to the other years (2009–2015), daily NEE in 2017 showed greater net carbon emissions during the first 4 months following the inundation (Figure 8a). Its value became negative (net CO_2 uptake) only at the end of the third month after inundation, which was ~2 months later than other years. After the fourth month following inundation, NEE tended to be more negative in 2017 than the other years. Similarly, NDVI was lower in 2017 than other years (2009–2015) within the first four postinundation months, and its value increased to a similar magnitude of other years only at the beginning of the fifth month (Figure 8b).

4 | DISCUSSION

This study has shown links between inundation and ecosystem CO_2 exchange rates in a freshwater wetland. To the best of our knowledge, this is the first study that has analyzed the effects of inundation
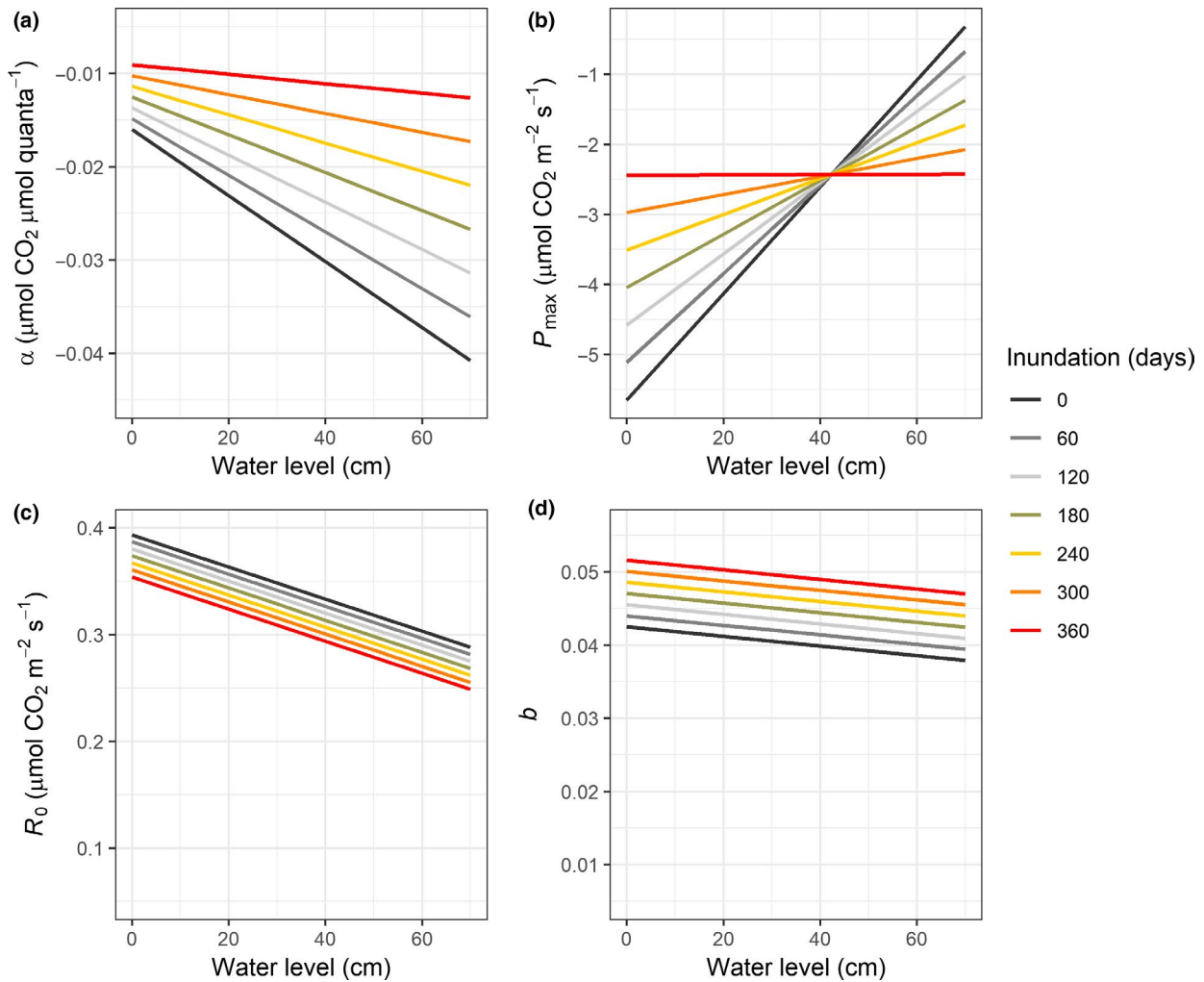
FIGURE 3 Parameters (a: α, b: P_{max}, c: R_0, and d: b) from the light response curve for gross primary production (GPP) and the temperature response curve for ecosystem respiration (ER) as a function of water level (WL) at different inundation durations (IDs). The relationships were determined based on least square mean predictions of the model with interaction terms between WL and ID for GPP in Table 2 and of the model without interaction terms for ER in Table S1
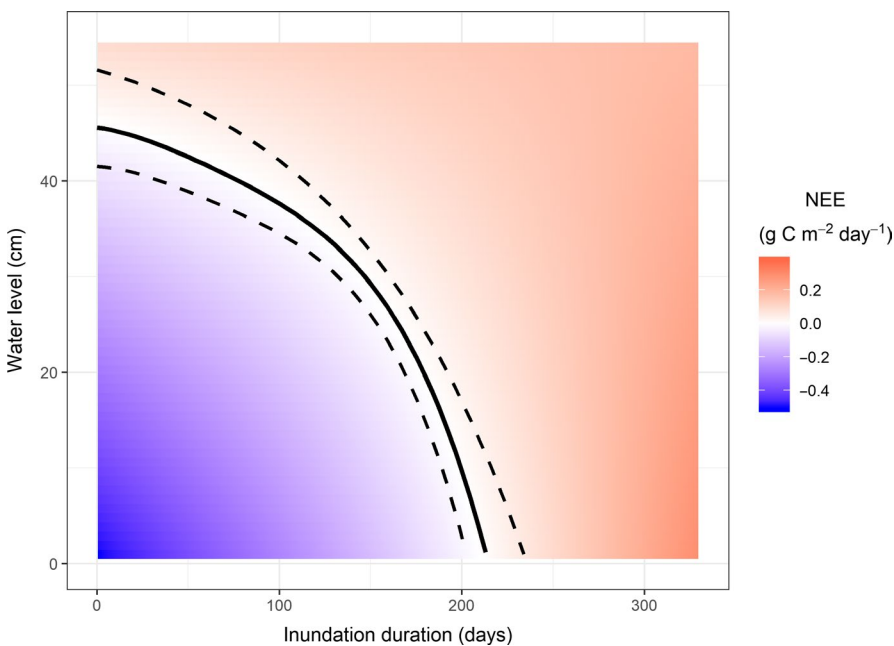

FIGURE 4 Net ecosystem CO_2 exchange (NEE) as a function of the interaction between WL and ID based on the least square mean predictions from the model in Table 2. The solid curve indicates the compensation points (i.e., NEE = 0 g C m^{-2} day^{-1}) under the corresponding conditions. The dashed lines represent the 95% confidence interval of the compensation points
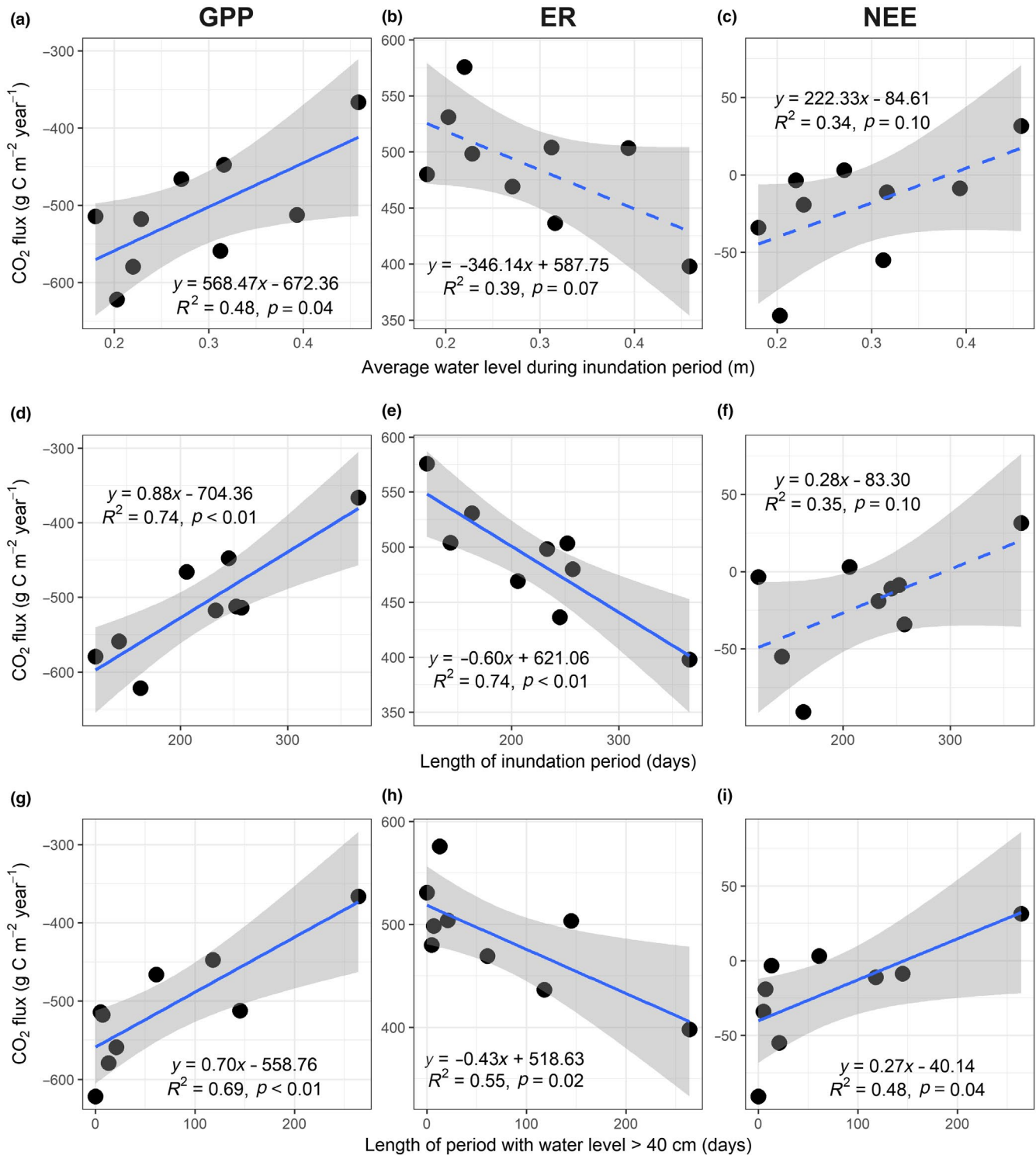
FIGURE 5 The sum of annual gross primary production (GPP) (a, d, g), ecosystem respiration (ER) (b, e, h) and net ecosystem CO_2 exchange (NEE) (c, f, i) as functions of average WL during the inundation period (a–c), length of inundation period (d–f), and length of the period with WL >40 cm each year (g–i). Solid lines indicate significant linear regressions ($p < 0.05$) and dashed lines indicate regressions are not significant ($p > 0.05$). Gray areas denote the 95% confidence intervals

as continuous variables (i.e., WL and ID), rather than as binary or discrete variables (i.e., inundated vs. noninundated or high vs. low WL), on NEE and its components (i.e., GPP and ER). Our study highlights that the combination of WL and ID is the main driver controlling the

annual CO_2 budget at the site. Importantly, with the influences of ENSO and water management activities, the extremely long ID and high WL that occurred in 2016 greatly restrained ecosystem CO_2 uptake, which shifted the wetland from what is typically CO_2 neutral or
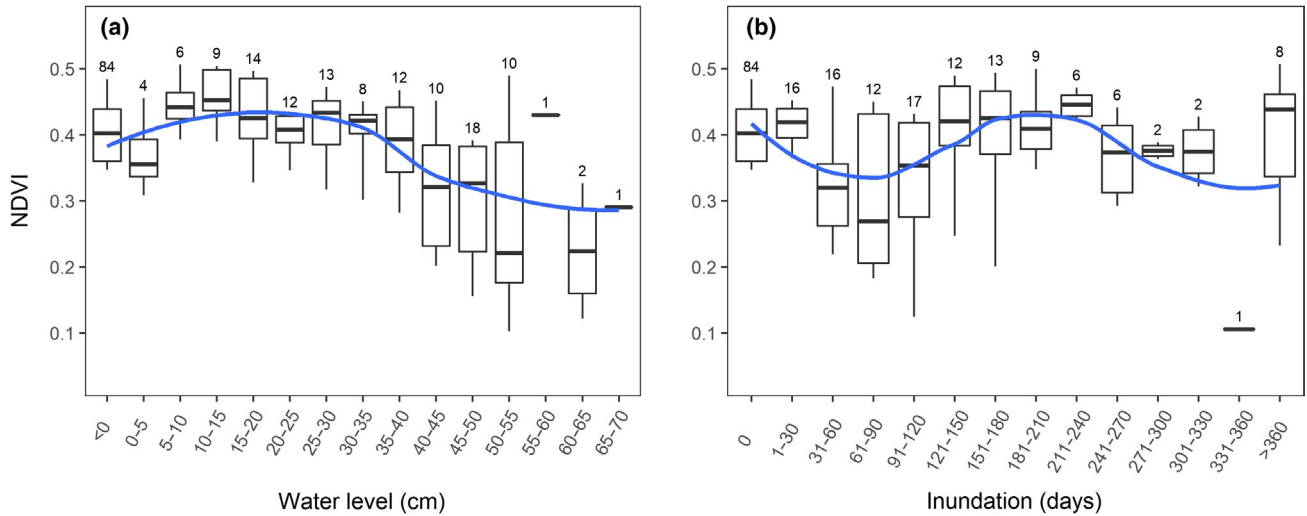
FIGURE 6 Bin-averages of the normalized difference vegetation index (NDVI) as functions of different water levels (a) and inundation durations (b) during 2008–2017. The bottom and top of a box indicate the values of lower and upper quartiles, respectively, and the horizontal line within the box is the median. The lower and upper whiskers represent the values of the 10th and 90th percentiles, respectively. The number of observations for each bin is shown above the corresponding box. Smooth lines in blue are added for visualizing the trend
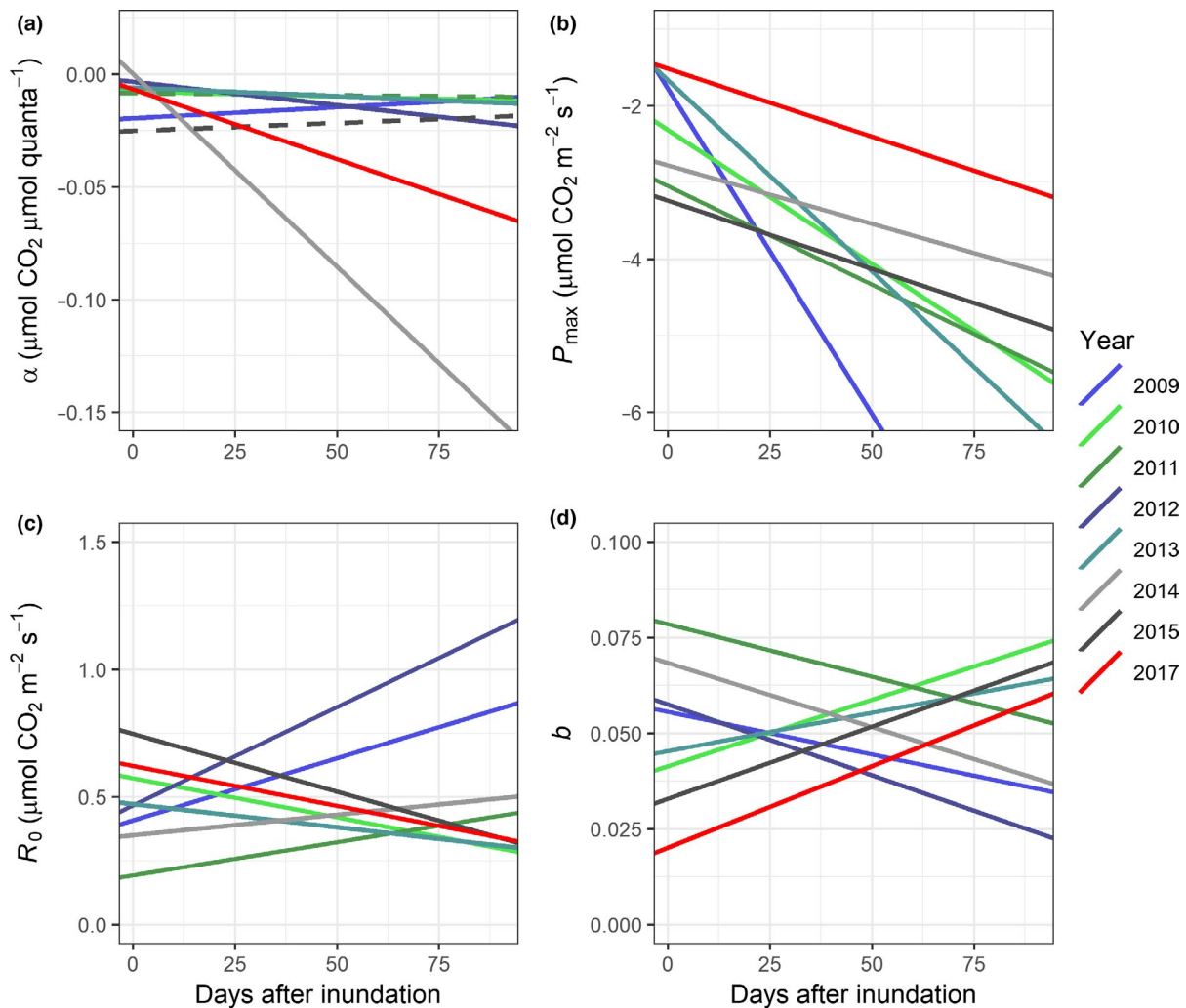
FIGURE 7 Estimated model parameters of light (α, a; P_{max}, b) and temperature (R_0, c; b, d) response curves as functions of the number of days after inundation in 2009–2017. Solid lines indicate slopes that are significantly different from zero ($p < 0.05$) while nonsignificant slopes are indicated by dashed lines ($p > 0.05$). The site was inundated year round in 2016 and no postinundation data are available for 2016
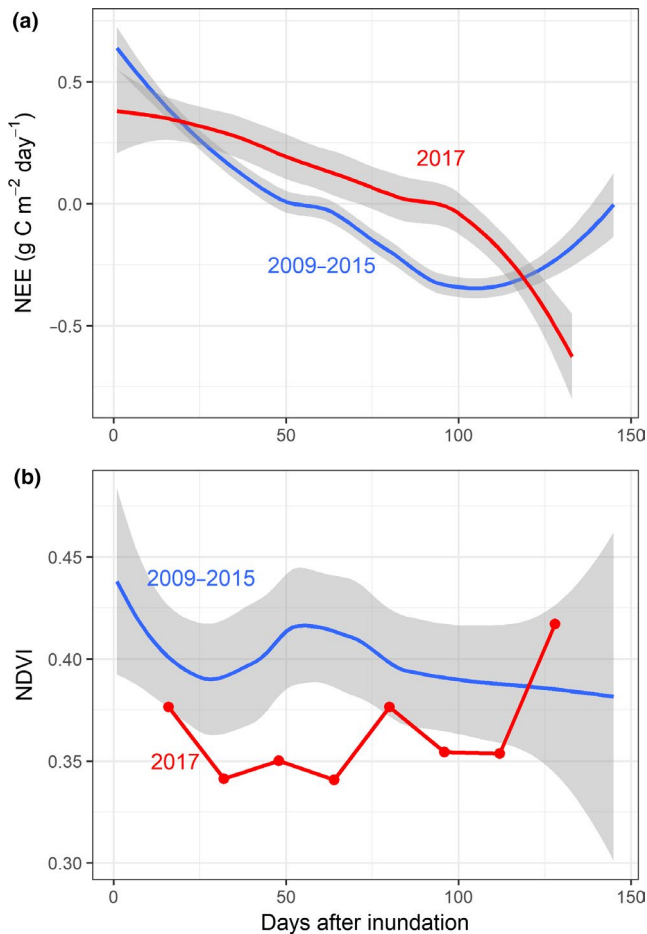
FIGURE 8 Postinundation variations in the net ecosystem CO_2 exchange (NEE; a) and normalized difference vegetation index (NDVI; b) in 2009–2015 (blue) and 2017 (red). The variations of the variables are represented by smooth lines based on Local Polynomial Regression (LOESS) with 95% confidence intervals (gray area). Individual data points of NDVI in 2017 are plotted due to the limited number of available data (<10). The site was inundated year round in 2016 and no postinundation data are present for 2016

a sink to a source. Considering that freshwater wetlands are net CO_2 sinks globally with an average NEE of -155 ± 31 g C m^{-2} $year^{-1}$ (Lu et al., 2016), our site with a NEE of -20.8 ± 11.8 g C m^{-2} $year^{-1}$ has a relatively weak carbon sink capacity. For such an ecosystem, an annual net loss of CO_2 induced by the extreme inundation could have a more critical impact on its carbon pool compared to those wetlands with a higher carbon sequestration capacity.

4.1 | Effects of inundation on GPP

Our results indicate that an increase in WL caused a decline in maximum ecosystem CO_2 uptake rate (P_{max}) (Figure 3b; Table 2). Theoretically, ecosystem CO_2 uptake is determined by the amount of photosynthetic tissue in the system and the photosynthetic rate of that tissue. At this site, macrophyte photosynthesis plays an important role in primary production (Schedlbauer, Munyon, Oberbauer, Gaiser, & Starr, 2012). An

increase in WL submerges the macrophyte leaves, which reduces the total amount of exposed leaf area in the ecosystem (Schedlbauer et al., 2010). This decline in photosynthetic leaf area was also supported by the associated decrease in NDVI (Figure 6a), which partially explained the relationship between P_{max} and WLs. Zhao, Olivas, et al. (2018) also found a substantial reduction in photosynthetic rates for the dominant plants (especially muhly grass, *M. filipes*) under inundation at the site. Therefore, we suggest that both the declines in photosynthetic leaf area and photosynthetic rates contributed to the decrease in ecosystem level P_{max} as WL increased.

At the same time, the effect of WL on P_{max} strongly depended on the ID (Table 2, Figure 3b), suggesting that the effect of WL is more noticeable under a short inundation period. An increase in ID can enhance the physiological stresses that are imposed by inundation and further decrease plant photosynthesis (Bragina et al., 2002; Chen et al., 2010). However, unlike GPP, NDVI was unaffected by ID changes (Table 2, Figure 6b), which may be due to the poor responses of the vegetation index to plant physiological changes (Huete et al., 2002; Running & Nemani, 1988), especially under inundation conditions. As inundation period exceeds 1 year, the effect of WL changes generally became minor because the plants were already severely stressed as indicated by the low P_{max}.

Overall, we suggest that enhanced inundation intensity (i.e., increase in WL and ID) decreases ecosystem CO_2 uptake by restraining the macrophyte photosynthesis and reducing the nonsubmerged photosynthetic leaf area. Nevertheless, this relationship can vary among ecosystems that are dominated by plant species with different inundation tolerance. For example, Jones, Stagg, Krauss, and Hester (2018) observed enhanced photosynthesis in *Spartina alterniflora*, a more inundation-tolerant plant, when exposed to a WL of ~10 cm. This increase of plant-level production may potentially enhance the ecosystem level net CO_2 uptake under a mild inundation. Therefore, more studies in different wetland ecosystems are still needed to develop a full understanding of the relationships between GPP and WL or ID.

4.2 | Effects of inundation on ER

The R_0 showed a decline as WL increased (Figure 3c, Table S1). Particularly, we found that this relationship tended to be nonlinear, where no obvious reduction in R_0 was present when WL increased beyond 30 cm (Figure S2, Table S3). While a decrease in soil heterotrophic respiration under anoxic conditions has been well-documented in previous studies (Anderson & Smith, 2002; Conner & Day, 1991; Fenner & Freeman, 2011; Happelll & Chanton, 1993), this nonlinear relationship between WL above the ground and ER has never been reported before. Inundation restrains heterotrophic respiration by reducing oxygen availability. Our result suggests that a WL of 30 cm may have minimized the available soil oxygen and greater WLs beyond this point may have a limited effect on available oxygen. In addition, aquatic metabolism also plays an important role in ecosystem CO_2 fluxes of

freshwater wetlands and these processes generally cause the water body in the ecosystem to be net heterotrophic (i.e., net CO_2 emission) (Hagerthey, Cole, & Kilbane, 2010). Increase in WL may potentially enhance the heterotrophic contribution from aquatic metabolism, which may dampen the overall decline of heterotrophic respiration at some points. Nevertheless, such nonlinear processes need to be considered in the ecosystem modeling.

Plant root respiration usually decreases with inundation due to oxygen limitation in the soil (Gleason & Dunn, 1982; Islam & Macdonald, 2004; Schlüter, Furch, & Joly, 1993), which may have also contributed to the decline of R_0 in this study. Unlike root respiration, leaf respiration usually decreases only when severe physiological stress develops and impedes the metabolism of the plants (Bradford, 1983; Gleason & Dunn, 1982; Liao & Lin, 1996). Some even observed a slight increase in leaf respiration under inundation stress (Chen et al., 2010). In this study, the duration of inundation showed no effect on ER, which may indicate that stress-induced changes in leaf respiration have only minor impacts on CO_2 emission at the ecosystem level.

Overall, our results indicate that inundation did reduce the rate of ER; however, a more intensive inundation (i.e., deeper and longer inundation) did not differ in its effect on the rate of ER from a mild inundation.

4.3 | Effects of inundation on NEE

Due to the unequal responses of GPP and ER, inundation weakened the net CO_2 sink strength of the ecosystem in our study, which is in line with research carried out in an episodically flooded wetland dominated by common reed (*Phragmites australis*) in China (Han et al., 2015). However, another study reported opposite results indicating that inundation enhanced the ecosystem CO_2 sink strength of a wetland dominated by Aleman grass (*Echinochloa polystachya*) in the Amazon floodplain (Morison et al., 2000). Based on our results, the changes in NEE under inundation were driven more by changes in GPP rather than ER, as ER was less responsive to high WLs (i.e., >30 cm) (Figure S2, Table S3) and prolonged inundation (Figure 3). Therefore, inundation tolerance of the dominant species and their photosynthetic responses, which drive the variations of GPP, can be important factors that control NEE in different wetland ecosystems (Larmola et al., 2004). Particularly, a wetland that is dominated by species with great inundation tolerance can be even more productive under moderate inundation (e.g., Morison et al., 2000).

Furthermore, we found the effect of WL on NEE is strengthened by the extension of inundation (Table 2, Figure 4). Based on the results, we suggest that the wetland became a net CO_2 source in 2016 because of a combination of high WLs and an extended inundation period. This conclusion is also supported by the interannual correlations between inundation intensity and CO_2 fluxes, where the greatest positive NEE (carbon loss) was associated with the longest period of WL >40 cm in 2016 (Figure 5i). Nevertheless, other wetland ecosystems that experience seasonal inundation may also have similar relationship

between NEE and WL/ID as shown in this study, but the compensation point that turns an ecosystem from CO_2 sink to source may differ among sites depending on the dominant plant species. This compensation point can be taken as an indicator for evaluating the vulnerability of a wetland to inundation. A site that has a low compensation point (i.e., at low WL or within a short inundation period) is more vulnerable to inundation while those having compensation points well beyond the normal range of maximum WL and ID are less likely to become a CO_2 source.

4.4 | Postinundation effects

As expected, the extreme inundation in 2016 was indeed followed by lower P_{max} (Figure 7) and a longer recovery period to resume the average net CO_2 uptake (i.e., as indicated by negative NEE) in 2017 compared to other years (Figure 8). Inevitably, this longer period of low P_{max} enhanced the annual CO_2 source capacity in 2017 (Figure 2d). Similar effect of extreme inundation has been reported for NEE in the following season in other wetland studies (Dušek et al., 2009; Hu et al., 2015). This reduction in P_{max} was related to slow plant physiological recovery from severe inundation stress that limited photosynthetic rates and new leaf development (Chen et al., 2010; Hu et al., 2015; Kozlowski & Pallardy, 1979). This explanation was also supported by the relatively low postinundation NDVI in 2017 (Figure 8). Even though this extreme inundation event influenced the CO_2 uptake rates of the following season, no significant correlations were present between inundation intensity and postinundation CO_2 fluxes across the studied years ($p > 0.05$, data not shown). Therefore, we suggest that inundation reduces the net ecosystem CO_2 uptake in the following dry season only when it leads to extraordinary physiological stress to or even death of the dominant plants. Interestingly, a greater ecosystem net CO_2 uptake was present after the recovering period (i.e., 4 months after the inundation) in 2017 than in other years. Whether this was a consequence of the extreme inundation event or the specific climatic conditions in 2017 is still not clear. Nevertheless, to better understand the processes underlying this cross-seasonal effect, future investigations on vegetation recovery associated with different stress levels caused by inundation and their relationship with ecosystem scale fluxes are needed.

4.5 | Implications for future hydrological changes

Everglades short-hydroperiod freshwater marl prairies are representative of wetlands with a regular seasonal inundation period of less than a year. Increases in WL and ID facilitated stronger declines in GPP than ER, and, consequently, a reduction in CO_2 sink strength. An extremely intensive inundation event eventually turned the ecosystem into a CO_2 source. Other freshwater wetlands that have regular inundation periods may exhibit similar responses of CO_2 fluxes to inundation depending on the inundation tolerance of the dominant

species. Given that extreme flooding occasions tend to keep increasing in many regions due to climate change (IPCC, 2013) or water management (e.g., Perry, 2004), we suggest that the carbon sink strength of the wetlands in these regions may be weakened, which would positively feedback to ongoing climate change. On the other hand, if inundation intensity remains high for longer periods, the vegetation in these systems can shift toward more inundation tolerant species within years (Armentano et al., 2006), which could further alter the relationship between CO_2 fluxes and inundation. Moreover, development of submerged photosynthetic capacity (e.g., from periphyton and submerged aquatic plants) over the long-term inundation may also partially compensate for reduced above water photosynthetic capacity under inundation. Our study reveals the relationships between the components of ecosystem CO_2 flux and inundation intensity, which are important for improving ecosystem and Earth-system models. However, the processes underlying the relationships and the long-term changes are largely unexplored. More studies that focus on macrophyte physiology, species composition, and aquatic carbon processes in response to inundation are still needed.

ORCID

Junbin Zhao https://orcid.org/0000-0001-5142-4901
Sparkle L. Malone https://orcid.org/0000-0001-9034-1076
Gregory Starr https://orcid.org/0000-0002-7918-242X

REFERENCES

Anderson, J. T., & Smith, L. M. (2002). The effect of flooding regimes on decomposition of *Polygonum pensylvanicum* in playa wetlands (Southern Great Plains, USA). *Aquatic Botany*, 74(2), 97–108. https://doi.org/10.1016/S0304-3770(02)00049-9

Armentano, T. V., Sah, J. P., Ross, M. S., Jones, D. T., Cooley, H. C., & Smith, C. S. (2006). Rapid responses of vegetation to hydrological changes in Taylor Slough, Everglades National Park, Florida, USA. *Hydrobiologia*, 569(1), 293–309. https://doi.org/10.1007/s10750-006-0138-8

Aubinet, M., Grelle, A., Ibrom, A., Rannik, Ü., Moncrieff, J., Foken, T., ... Vesala, T. (2000). Estimates of the annual net carbon and water exchange of forests: The EUROFLUX methodology. *Advances in Ecological Research*, 30(C), 113–175. https://doi.org/10.1016/S0065-2504(08)60018-5

Baldocchi, D. D., Hicks, B. B., & Meyers, T. P. (1988). Measuring biosphere-atmosphere exchanges of biologically related gases with micrometeorological methods. *Ecology*, 69(5), 1331–1340. https://doi.org/10.2307/1941631

Bradford, K. J. (1983). Effects of soil flooding on leaf gas exchange of tomato plants. *Plant Physiology*, 73(2), 475–479. https://doi.org/10.1104/pp.73.2.475

Bragina, T. V., Drozdova, I. S., Ponomareva, Y., Alekhin, V. I., & Grineva, G. M. (2002). Photosynthesis, respiration, and transpiration in maize seedlings under hypoxia induced by complete flooding. *Doklady Biological Sciences*, 384(6), 274–277.

Burkett, V., & Kusler, J. (2000). Climate change: Potential impacts and interactions in wetlands of United States. *Journal of the American Water Resources Association*, 36(2), 313–320. https://doi.org/10.1111/j.1752-1688.2000.tb04270.x

Canty, A., & Ripley, B. (2017). boot: Bootstrap R (S-Plus) functions. R package version 1.3-20.

Chen, H., Zamorano, M. F., & Ivanoff, D. (2010). Effect of flooding depth on growth, biomass, photosynthesis, and chlorophyll fluorescence of *Typha domingensis*. *Wetlands*, 30(5), 957–965. https://doi.org/10.1007/s13157-010-0094-y

Childers, D. L., Iwaniec, D., Rondeau, D., Rubio, G., Verdon, E., & Madden, C. J. (2006). Responses of sawgrass and spikerush to variation in hydrologic drivers and salinity in Southern Everglades marshes. *Hydrobiologia*, 569(1), 273–292. https://doi.org/10.1007/s10750-006-0137-9

Conner, W. H., & Day, J. W. (1991). Leaf litter decomposition in three Louisiana freshwater forested wetland areas with different flooding regimes. *Wetlands*, 11(2), 303–312. https://doi.org/10.1007/BF03160855

Davis, S. M., & Ogden, J. C. (1994). *Everglades, the ecosystem and its restoration*. Delray Beach, FL: St. Lucie Press.

Didan, K. (2015). MYD13Q1 MODIS/aqua vegetation indices 16-day L3 global 250m SIN grid V006. *NASA EOSDIS Land Processes DAAC*. https://doi.org/10.5067/MODIS/MYD13Q1.006

Dušek, J., Čížková, H., Czerný, R., Taufarová, K., Šmídová, M., & Janouš, D. (2009). Influence of summer flood on the net ecosystem exchange of CO_2 in a temperate sedge-grass marsh. *Agricultural and Forest Meteorology*, 149(9), 1524–1530. https://doi.org/10.1016/j.agrformet.2009.04.007

Erwin, K. L. (2009). Wetlands and global climate change: The role of wetland restoration in a changing world. *Wetlands Ecology and Management*, 17(1), 71–84. https://doi.org/10.1007/s11273-008-9119-1

Fenner, N., & Freeman, C. (2011). Drought-induced carbon loss in peatlands. *Nature Geoscience*, 4(12), 895–900. https://doi.org/10.1038/ngeo1323

Gleason, M. L., & Dunn, E. L. (1982). Effects of hypoxia on root and shoot respiration of *Spartina alterniflora*. In V. S. Kennedy (Ed.), *Estuarine comparisons* (pp. 243–253). Gleneden Beach, OR: Academic Press. https://doi.org/10.1016/B978-0-12-404070-0.50020-X

Goulden, M. L., Munger, W., Fan, S., Daube, B. C., & Wofsy, S. C. (1996). Measurements of carbon sequestration by long-term eddy covariance: Methods and a critical evaluation of accuracy. *Global Change Biology*, 2, 169–182. https://doi.org/10.1111/j.1365-2486.1996.tb00070.x

Hagerthey, S. E., Cole, J. J., & Kilbane, D. (2010). Aquatic metabolism in the Everglades: Dominance of water column heterotrophy. *Limnology and Oceanography*, 55(2), 653–666. https://doi.org/10.4319/lo.2009.55.2.0653

Han, G., Chu, X., Xing, Q., Li, D., Yu, J., Luo, Y., ... Rafique, R. (2015). Effects of episodic flooding on the net ecosystem CO_2 exchange of a supratidal wetland in the Yellow River Delta. *Journal of Geophysical Research: Biogeosciences*, 120, 1506–1520. https://doi.org/10.1002/2014JG002797.Received

Happelll, D., & Chanton, P. (1993). Carbon remineralization in a north Florida swamp forest: Effects of water level on the pathways and rates of soil organic matter decomposition. *Global Bioceochemical Cycles*, 7(3), 475–490. https://doi.org/10.1029/93GB00876

Hollinger, A. D. Y., Kelliher, F. M., Byers, J. N., Hunt, J. E., Mcseveny, T. M., & Weir, L. (1994). Carbon dioxide exchange between an undisturbed old-growth temperate forest and the atmosphere. *Ecology*, 75(1), 134–150. https://doi.org/10.2307/1939390

Hu, Q., Wu, Q., Yao, B., & Xu, X. (2015). Ecosystem respiration and its components from a Carex meadow of Poyang Lake during the drawdown period. *Atmospheric Environment*, 100, 124–132. https://doi.org/10.1016/j.atmosenv.2014.10.047

Huete, A., Didan, K., Miura, H., Rodriguez, E. P., Gao, X., & Ferreira, L. F. (2002). Overview of the radiometric and biopyhsical performance of the MODIS vegetation indices. *Remote Sensing of Environment*, 83, 195–213.

IPCC. (2013). *Climate change 2013: The physical science basis*. Contribution of Working Group I to the Fifth Assessment Report of the Intergovernmental Panel on Climate Change. Cambridge, UK and New York, NY: Cambridge University Press. https://doi.org/10.1017/CBO9781107415324

Islam, M. A., & Macdonald, S. E. (2004). Ecophysiological adaptations of black spruce (*Picea mariana*) and tamarack (*Larix laricina*) seedlings to flooding. *Trees - Structure and Function*, 18(1), 35–42. https://doi.org/10.1007/s00468-003-0276-9

Jimenez, K. L., Starr, G., Staudhammer, C. L., Schedlbauer, J. L., Loescher, H. W., Malone, S. L., & Oberbauer, S. F. (2012). Carbon dioxide exchange rates from short- and long-hydroperiod Everglades freshwater marsh. *Journal of Geophysical Research: Biogeosciences*, 117(4), 1–17. https://doi.org/10.1029/2012JG002117

Jones, S. F., Stagg, C. L., Krauss, K. W., & Hester, M. W. (2018). Flooding alters plant-mediated carbon cycling independently of elevated atmospheric CO_2 concentrations. *Journal of Geophysical Research: Biogeosciences*, 123, 1976–1987. https://doi.org/10.1029/2017JG004369

Kayranli, B., Scholz, M., Mustafa, A., & Hedmark, Å. (2010). Carbon storage and fluxes within freshwater wetlands: A critical review. *Wetlands*, 30(1), 111–124. https://doi.org/10.1007/s13157-009-0003-4

Kozlowski, T. T. (1984). Plant responses to flooding of soil. *BioScience*, 34(3), 162–167. https://doi.org/10.2307/1309751

Kozlowski, T. T., & Pallardy, S. G. (1979). Stomatal responses of *Fraxinus pennsylvanica* seedlings during and after flooding. *Physiologia Plantarum*, 46(2), 155–158. https://doi.org/10.1111/j.1399-3054.1979.tb06549.x

Larmola, T., Alm, J., Juutinen, S., Saarnio, S., Martikainen, P. J., & Silvola, J. (2004). Floods can cause large interannual differences in littoral net ecosystem productivity. *Limnology and Oceanography*, 49(5), 1896–1906. https://doi.org/10.4319/lo.2004.49.5.1896

Liao, C. T., & Lin, C. H. (1996). Photosynthetic responses of grafted bitter melon seedlings to flood stress. *Environmental and Experimental Botany*, 36(2), 167–172. https://doi.org/10.1016/0098-8472(96)01009-X

Lu, W., Xiao, J., Liu, F., Zhang, Y., Liu, C., & Lin, G. (2016). Contrasting ecosystem CO_2 fluxes of inland and coastal wetlands: A meta-analysis of eddy covariance data. *Global Change Biology*, 1180–1198, https://doi.org/10.1111/gcb.13424

Malone, S. L., Starr, G., Staudhammer, C. L., & Ryan, M. G. (2013). Effects of simulated drought on the carbon balance of Everglades short-hydroperiod marsh. *Global Change Biology*, 19(8), 2511–2523. https://doi.org/10.1111/gcb.12211

Malone, S. L., Staudhammer, C. L., Loescher, H. W., Olivas, P., Oberbauer, S. F., Ryan, M. G., ... Starr, G. (2014). Seasonal patterns in energy partitioning of two freshwater marsh ecosystems in the Florida Everglades. *Journal of Geophysical Research: Biogeosciences*, 119(8), 1487–1505. https://doi.org/10.1002/2014jg002700

Malone, S. L., Staudhammer, C. L., Oberbauer, S. F., Olivas, P., Ryan, M. G., Schedlbauer, J. L., ... Starr, G. (2014). El Nino Southern Oscillation (ENSO) enhances CO_2 exchange rates in freshwater marsh ecosystems in the Florida everglades. *PLoS ONE*, 9(12), e115058. https://doi.org/10.1371/journal.pone.0115058

Morison, J. I. L., Piedade, M. T. F., Müller, E., Long, S. P., Junk, W. J., & Jones, M. B. (2000). Very high productivity of the C_4 aquatic grass *Echinochloa polystachya* in the Amazon floodplain confirmed by net ecosystem CO_2 flux measurements. *Oecologia*, 125(3), 400–411. https://doi.org/10.1007/s004420000464

Perry, W. (2004). Elements of South Florida's comprehensive everglades restoration plan. *Ecotoxicology*, 13(3), 185–193. https://doi.org/10.1023/B:ECTX.0000023564.10311.4a

Pezeshki, S. R. (2001). Wetland plant responses to soil flooding. *Environmental and Experimental Botany*, 46(3), 299–312. https://doi.org/10.1016/S0098-8472(01)00107-1

Pinheiro, J., Bates, D., DebRoy, S., & Sarkar, D.; R Development Core Team. (2013). nlme: Linear and nonlinear mixed effects models. R package version 3.1-108.

R Development Core Team. (2018). *R: A language and environment for statistical computing*. Vienna, Austria: R Foundation for Statistical Computing. Retrieved from http://www.R-project.org/

Rocha, A. V., & Goulden, M. L. (2010). Drought legacies influence the long-term carbon balance of a freshwater marsh. *Journal of Geophysical Research: Biogeosciences*, 115, G00H02. https://doi.org/10.1029/2009JG001215

Running, S. W., & Nemani, R. R. (1988). Relating seasonal patterns of the AVHRR vegetation index to simulated photosynthesis and transpiration of forests in different climates. *Remote Sensing of Environment*, 24(2), 347–367. https://doi.org/10.1016/0034-4257(88)90034-X

Schaffranek, R. W., & Ball, M. H. (2000). Flow velocities in wetlands adjacent to canal C-111 in south Florida. In J. R. Eggleston, T. L. Embry, R. H. Mooney, L. Wedderburn, C. R. Goodwin, H. S. Hinkel, K. M. Pegram, and T. J. Enright (Compilers), US Geological Survey Program on the South Florida Ecosystem: 2000 Proceedings: Presentations Made at the Greater Everglades Rest, 45–47.

Schedlbauer, J. L., Munyon, J. W., Oberbauer, S. F., Gaiser, E. E., & Starr, G. (2012). Controls on ecosystem carbon dioxide exchange in short- and long-hydroperiod Florida everglades freshwater marshes. *Wetlands*, 32(5), 801–812. https://doi.org/10.1007/s13157-012-0311-y

Schedlbauer, J. L., Oberbauer, S. F., Starr, G., & Jimenez, K. L. (2010). Seasonal differences in the CO_2 exchange of a short-hydroperiod Florida Everglades marsh. *Agricultural and Forest Meteorology*, 150(7–8), 994–1006. https://doi.org/10.1016/j.agrformet.2010.03.005

Schlüter, U. B., Furch, B., & Joly, C. A. (1993). Physiological and anatomical adaptations by young *Astrocaryum jauari* Mart. (Arecaceae) in periodically inundated biotopes of central Amazonia. *Biotropica*, 25(4), 384–396.

Taylor, S. H., Ripley, B. S., Woodward, F. I., & Osborne, C. P. (2011). Drought limitation of photosynthesis differs between C_3 and C_4 grass species in a comparative experiment. *Plant, Cell and Environment*, 34(1), 65–75. https://doi.org/10.1111/j.1365-3040.2010.02226.x

Todd, M. J., Muneepeerakul, R., Pumo, D., Azaele, S., Miralles-Wilhelm, F., Rinaldo, A., & Rodriguez-Iturbe, I. (2010). Hydrological drivers of wetland vegetation community distribution within Everglades

National Park, Florida. *Advances in Water Resources, 33*(10), 1279–1289. https://doi.org/10.1016/j.advwatres.2010.04.003

Webb, E. K., Pearman, G., & Leuning, R. (1980). Correction of flux measurements for density effects due to heat and water vapour transfer. *Quarterly Journal of the Royal Meteorological Society, 106*, 85–100. https://doi.org/10.1002/qj.49710644707

Wickham, H. (2016). *ggplot2: Elegant graphics for data analysis.* New York, NY: Springer-Verlag.

Zhao, J., Oberbauer, S. F., Olivas, P. C., Schedlbauer, J. L., May, J. L., Moser, J. G., ... Starr, G. (2018). Contrasting photosynthetic responses of two dominant macrophyte species to seasonal inundation in an Everglades freshwater prairie. *Wetlands, 38*(5), 893–903. https://doi.org/10.1007/s13157-018-1038-1

Zhao, J., Olivas, P. C., Kunwor, S., Malone, S. L., Staudhammer, C. L., Starr, G., & Oberbauer, S. F. (2018). Comparison of sensible heat flux measured by large aperture scintillometer and eddy covariance in a seasonally-inundated wetland. *Agricultural and Forest Meteorology, 259*, 345–354. https://doi.org/10.1016/j.agrformet.2018.05.026

Zona, D., Lipson, D. A., Paw U, K. T., Oberbauer, S. F., Olivas, P., Gioli, B., & Oechel, W. C. (2012). Increased CO_2 loss from vegetated drained lake tundra ecosystems due to flooding. *Global Biogeochemical Cycles, 26*(2), 1–16. https://doi.org/10.1029/2011GB004037

SUPPORTING INFORMATION

Additional supporting information may be found online in the Supporting Information section at the end of the article.